Increased expression of AT-1/SLC33A1 causes an autistic-like phenotype in mice by affecting dendritic branching and spine formation

Rikki Hullinger,[1,2]* Mi Li,[1]* Jingxin Wang,[2,3] Yajing Peng,[1] James A. Dowell,[4] Ewa Bomba-Warczak,[2,5,6] Heather A. Mitchell,[7] Corinna Burger,[8] Edwin R. Chapman,[5,6] John M. Denu,[4] Lingjun Li,[3] and Luigi Puglielli[1,5,9]

[1]Department of Medicine, [2]Neuroscience Training Program, [3]School of Pharmacy and Department of Chemistry, [4]Department of Biomolecular Chemistry and the Wisconsin Institute for Discovery, [5]Department of Neuroscience, [6]Howard Hughes Medical Institute, [7]Rodent Models Core, Waisman Center, and [8]Department of Neurology, University of Wisconsin-Madison, Madison, WI 53705
[9]Geriatric Research Education Clinical Center, Veterans Affairs Medical Center, Madison, WI 53705

The import of acetyl-CoA into the lumen of the endoplasmic reticulum (ER) by AT-1/SLC33A1 regulates Nε-lysine acetylation of ER-resident and -transiting proteins. Specifically, lysine acetylation within the ER appears to influence the efficiency of the secretory pathway by affecting ER-mediated quality control. Mutations or duplications in *AT-1/SLC33A1* have been linked to diseases such as familial spastic paraplegia, developmental delay with premature death, and autism spectrum disorder with intellectual disability. In this study, we generated an AT-1 Tg mouse model that selectively overexpresses human AT-1 in neurons. These animals demonstrate cognitive deficits, autistic-like social behavior, aberrations in synaptic plasticity, an increased number of dendritic spines and branches, and widespread proteomic changes. We also found that AT-1 activity regulates acetyl-CoA flux, causing epigenetic modulation of the histone epitope H3K27 and mitochondrial adaptation. In conclusion, our results indicate that increased expression of AT-1 can cause an autistic-like phenotype by affecting key neuronal metabolic pathways.

The Journal of Experimental Medicine

Acetyl-CoA is an essential substrate for a wide range of biochemical reactions that occur within the cell (Pietrocola et al., 2015). Cytosolic acetyl-CoA is produced predominantly by the conversion of citrate and coenzyme A (CoA) by ATP-citrate lyase (ACLY) and the condensation of free acetate and CoA by acetyl-CoA synthetase (ACESS2, also referred to as AceCS; Pehar and Puglielli, 2013; Shi and Tu, 2015). Acetyl-CoA is then actively imported into the lumen of the ER by the ER membrane transporter AT-1 (also referred to as SLC33A1; Jonas et al., 2010), where it serves as donor of the acetyl group in the Nε-lysine acetylation of ER-resident and -transiting proteins (Choudhary et al., 2009; Pehar et al., 2012b).

Recent reports suggest that lysine acetylation within the ER is required for ER-mediated quality control. Specifically, the ER-based acetyltransferases ATase1 and ATase2 associate with the oligosaccharyl transferase complex to acetylate properly folded glycoproteins (Ding et al., 2014). In addition, studies performed with two type I membrane proteins indicate that the acetylation status of nascent secretory proteins in the ER regulates the efficiency of transport along the secretory pathway (Costantini et al., 2007; Mak et al., 2014).

Decreased influx of acetyl-CoA into the ER lumen leads to aberrant induction of autophagy in both cell-based (Jonas et al., 2010; Pehar et al., 2012a) and animal (Peng et al., 2014) models. At the mechanistic level, the induction of autophagy is linked to the acetylation status of autophagy-related protein 9A (Pehar et al., 2012a; Peng et al., 2014). Haploinsufficiency of AT-1 in the animal results in neurodegeneration, inflammation, and propensity to infections and cancer (Peng et al., 2014). Heterozygous mutations in AT-1 have been identified in patients affected by an autosomal dominant form of spastic paraplegia (Lin et al., 2008), whereas homozygous mutations have been identified in patients affected by severe developmental delay and childhood death (Huppke et al., 2012). Chromosomal duplications affecting the 3q25.31 locus harboring *AT-1/SLC33A1* have been associated with autism spectrum disorder (ASD) and intellectual disability (SFARI Autism Database; http://sfari.org/; Sanders et al., 2011; Prasad et al., 2012; Krumm et al., 2013). Additionally, a gain of ∼1.1–1.5 Mb in 3q25.2-3q25.31, which contained *AT-1/SLC33A1*

*R. Hullinger and M. Li contributed equally to this paper.

Correspondence to Luigi Puglielli: lp1@medicine.wisc.edu

Abbreviations used: AceCS, acetyl-CoA synthetase 2; ACLY, ATP-citrate lyase; ASD, autism spectrum disorder; AT-1, acetyl-CoA transporter 1; CoA, Coenzyme A; FC, fear conditioning; LTD, long-term depression; LTP, long-term potentiation; ManNaz, azide-modified mannosamine; MEF, mouse embryo fibroblasts; MWM, Morris water maze; NOR, novel object recognition; OPP, O-propargyl-puromycin; TBS, theta burst stimulation.

The Rockefeller University Press $30.00
J. Exp. Med. 2016 Vol. 213 No. 7 1267–1284
www.jem.org/cgi/doi/10.1084/jem.20151776

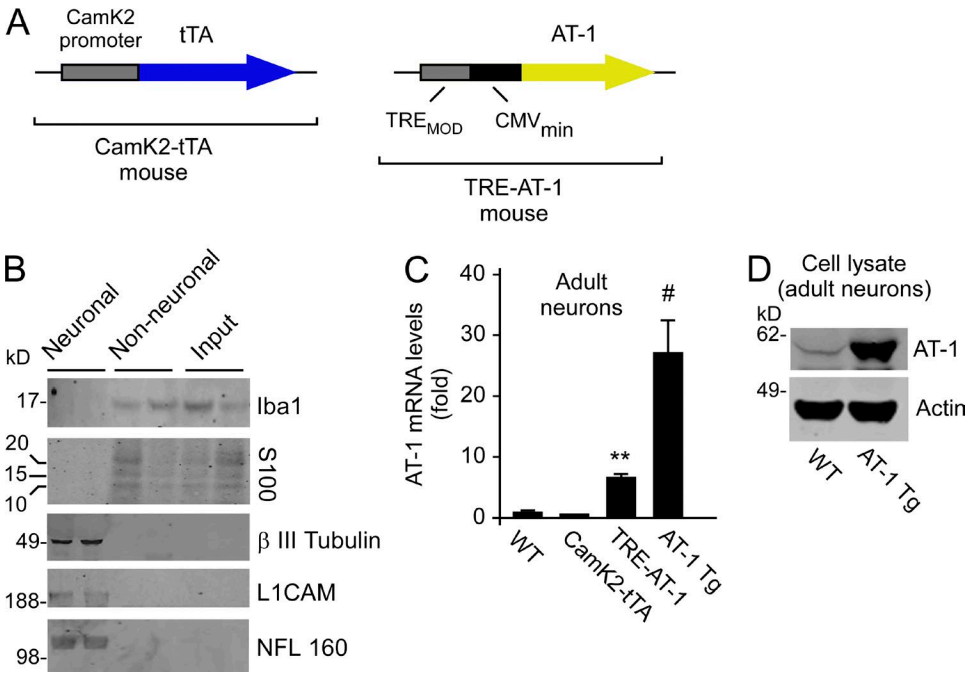

Figure 1. **AT-1 Tg mice selectively overexpress AT-1 in forebrain neurons.** (A) AT-1 Tg mice were generated with an inducible neuron-specific overexpression Tet-Off system driven by the CamK2 promoter. (B) Western blot showing isolation of neurons from the brain of adult AT-1 Tg mice. Total cells dissociated from the brain (Input), neuronal, and nonneuronal fractions are shown. The following markers were used: Iba1 for microglia; S100 for astrocytes; βIII Tubulin, L1CAM, and NFL 160 for neurons. (C and D) mRNA (C) and protein (D) levels of AT-1 in AT-1 Tg mice. Data in C represent three independent determinations of seven mice/group. **, $P < 0.005$; #, $P < 0.0005$. Student's *t* test and one-way ANOVA, followed by Tukey-Kramer multiple comparisons test. Bars represent mean ± SD.

and *Guanine Monphosphate Synthase* (*GMPS*, associated with myeloid leukemia) was found in three male children with autism, seizure, abnormal electroencephalogram, and facial dysmorphism (Swisshelm, K., et al. 2014. ASHG Annual Meeting; Abstract 3205T).

In this study, we sought to investigate the consequences of increased AT-1 activity. Specifically, we generated an AT-1 transgenic (Tg) mouse model that selectively overexpresses human AT-1 in neurons. These animals demonstrate cognitive deficits, autistic-like social behavior, aberrations in synaptic plasticity, increased number of dendritic spines and branches, and widespread proteomic changes. The synaptic phenotype appears to be caused by increased trafficking of nascent proteins along the secretory pathway. In addition, we found that AT-1 Tg animals display increased expression of mitochondrial enzymes related to acetyl-CoA production, suggesting that increased movement of acetyl-CoA into the ER causes downstream compensatory mechanisms in mitochondrial activity. Furthermore, this apparent mitochondrial adaptation appears to be driven by changes in the acetylation/methylation status of Lys27 on the histone protein H3 suggesting that this site acts as a sensor to adapt supply of citrate from the mitochondria to rapidly compensate for changes in cytosolic acetyl-CoA, as induced by increased AT-1 activity.

In conclusion, our results indicate that increased expression of AT-1 can cause an autistic-like phenotype by affecting key neuronal metabolic pathways.

RESULTS

AT-1 Tg animals display cognitive deficits and autistic-like behaviors

To explore the role of AT-1 in the brain, we generated Tg mice with an inducible neuron-specific overexpression Tet-Off system driven by the CamK2 promoter (Fig. 1 A). For the purpose of this study, the animals (referred to as AT-1 Tg) were maintained in the absence of doxycycline (Dox); as such, they overexpressed human AT-1 during development, as well as after birth. Direct assessment of both mRNA and protein levels in neurons isolated from the adult brain confirmed successful up-regulation of AT-1 in Tg mice (Fig. 1, B–D).

To determine whether selective overexpression of AT-1 in neurons would impact learning and memory, mice were assessed with the fear conditioning (FC), novel object recognition (NOR), and Morris water maze (MWM) tasks. We found that AT-1 Tg animals displayed significant deficits in each of these hippocampus-dependent tasks (Fig. 2, A–F). Specifically, we observed significant impairments in contextual FC (Fig. 2 A) and NOR (Fig. 2 B). The animals did not display differences in freezing behavior during the initial

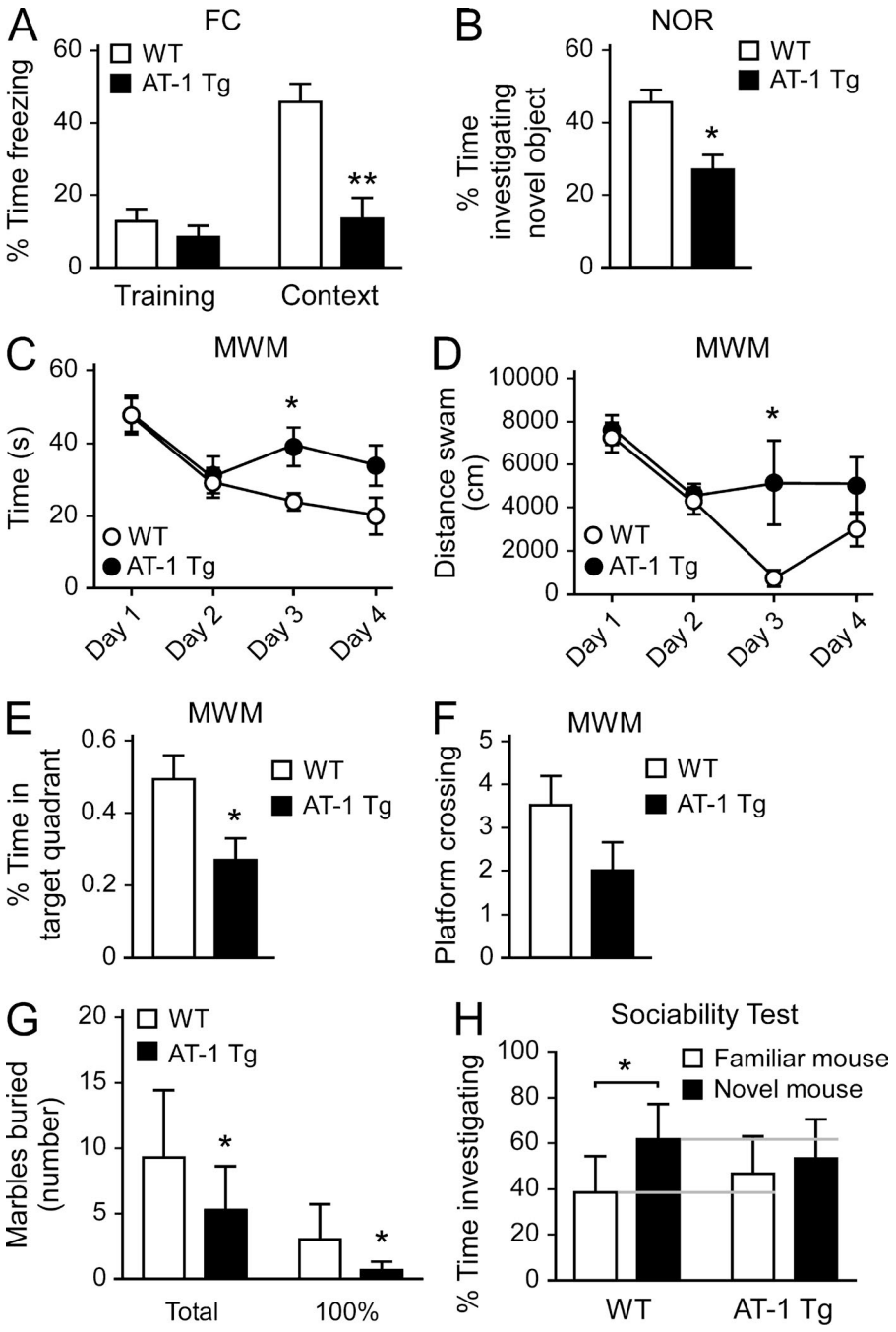

Figure 2. **AT-1 Tg animals display cognitive deficits and autistic-like social behaviors.** (A) Contextual FC. (WT, $n = 6$; AT-1 Tg, $n = 6$). (B) NOR (WT, $n = 11$; AT-1 Tg, $n = 12$). (C–F) MWM (WT, $n = 10$; AT-1 Tg, $n = 10$). (G) Marble burying task (WT, $n = 13$; AT-1 Tg, $n = 13$). Number of marbles that were at least 50% covered (total) and number of marbles that were completely buried (100%) are shown. (H) Social interaction test. Preference for investigating novel versus familiar mouse is shown. (WT, $n = 13$; AT-1 Tg, $n = 13$). *, $P < 0.05$; **, $P < 0.005$. Student's *t* test and one-way ANOVA, followed by Tukey-Kramer multiple comparisons test. Bars represent mean ± SD.

exposure to the behavior arena (Fig. 2 A, Training) and did not display increased anxiety in the open field test (unpublished data). In the NOR test, WT mice spent >40% of their total investigation time exploring the novel object, whereas AT-1 Tg mice displayed no preference for the novel object relative to the trained objects. During the training phase of the MWM task, Tg mice had a significantly higher escape latency (Fig. 2 C) and swam greater distances before locating the hidden platform than WT controls (Fig. 2 D). Furthermore, they spent less time in the target quadrant (Fig. 2 E) and displayed fewer platform crossings during the probe trial than WT animals (Fig. 2 F).

Given the possible association of *AT-1/SLC33A1* with ASD and intellectual disability, we decided to test AT-1 Tg mice with the marble burying and social preference paradigms, two commonly used models of autistic behavior. We found that Tg mice displayed decreased repetitive behavior in the marble burying task (Fig. 2 G) and failed to show a preference for investigating the novel mouse in the social preference paradigm (Fig. 2 H). These tests indicate aberrations

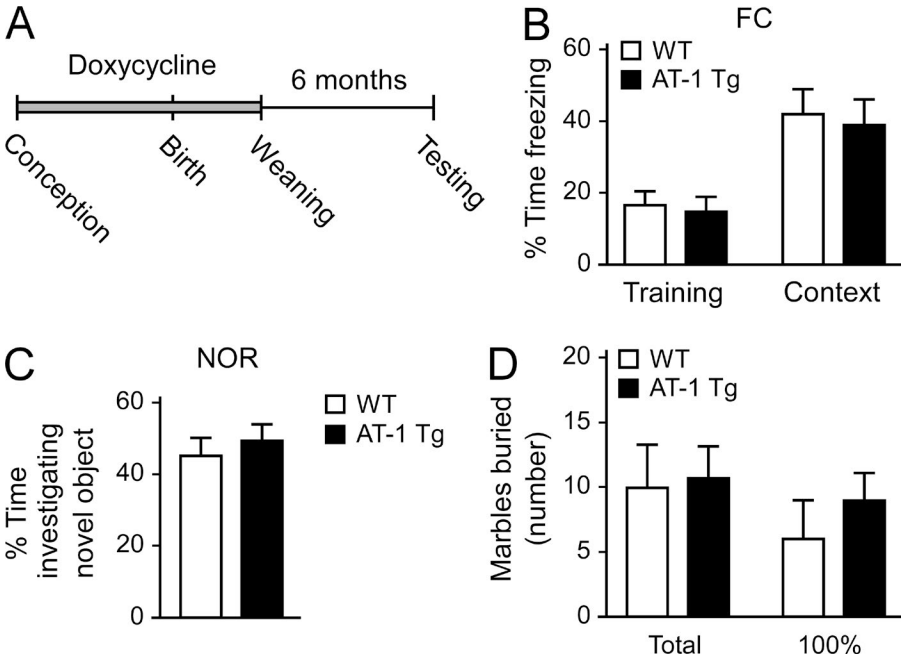

Figure 3. **Repression of AT-1 by Dox prevents cognitive deficits and autistic-like social behaviors.** (A) Schematic view of the experimental setting. Mice were tested 6 mo after suspension of Dox and induction of AT-1. (B) Contextual FC of Dox-treated AT-1 Tg mice (WT, $n = 12$; AT-1 Tg, $n = 12$). (C) NOR of Dox-treated AT-1 Tg mice (WT, $n = 12$; AT-1 Tg, $n = 12$). (D) Marble burying task of Dox-treated AT-1 Tg mice (WT, $n = 13$; AT-1 Tg, $n = 12$). Number of marbles that were at least 50% covered (total) and number of marbles that were completely buried (100%) are shown. Student's *t* test and one-way ANOVA, followed by Tukey-Kramer multiple comparisons test. Bars represent mean ± SD.

in repetitive behavior and social tendencies, suggesting that our Tg mouse line shares similarities with behavioral models of ASD (Gkogkas et al., 2013; Kouser et al., 2013; Dere et al., 2014; Lugo et al., 2014; Pucilowska et al., 2015; Speed et al., 2015). To assess whether the aforementioned behavioral changes were solely the result of developmental events, we also generated AT-1 Tg mice in the presence of Dox to repress expression of the transgene. The Dox was suspended at weaning and the animals were analyzed 6 mo later (Fig. 3 A). Under these conditions, we did not observe any differences with WT mice (Fig. 3, B–D), indicating that the aberrations in repetitive behavior and social tendencies described in Fig. 2 are solely—or mostly—developmental.

Although there is no specific behavioral profile that defines ASD in the mouse, the combined deficiency in FC, NOR, MWM, marble burying, and social preference paradigms observed in AT-1 Tg mice has been described in other mouse models of ASD (Gkogkas et al., 2013; Kouser et al., 2013; Dere et al., 2014; Lugo et al., 2014; Pucilowska et al., 2015; Speed et al., 2015). Because chromosomal duplications of the 3q25.31 locus, which harbors *AT-1/SLC33A1*, have been associated with ASD and intellectual disability (see later in the Discussion section), we conclude that AT-1 Tg mice display an autistic-like phenotype.

Tg mice demonstrate changes in neuronal morphology and aberrant synaptic plasticity

We next sought to investigate whether increased expression of AT-1 in neurons would lead to morphological and/or synaptic changes that could explain the behavioral phenotype. We found that cultured neurons from AT-1 Tg mice displayed a drastic increase in the number of dendritic branches and spines compared with WT controls (Fig. 4, A–D). Similar results were obtained in vivo by analyzing hippocampal tissue from 6-mo-old mice (Fig. 4 E), thus confirming that overexpression of AT-1 causes drastic changes in neuronal morphology.

Alterations in neuronal function were assessed by hippocampal slice electrophysiology. Long-term potentiation (LTP) and its counterpart, long-term depression (LTD), are believed to be correlated with cognitive function, and it is has been demonstrated that a balance between LTP and LTD must be present in order for normal learning and memory formation to occur (Feldman, 2009; Huganir and Nicoll, 2013). We found that AT-1 Tg mice display increased levels of hippocampal LTP elicited by Theta burst stimulation (3xTBS; Fig. 4 F) and significantly reduced LTD induced by paired pulse low-frequency facilitation (Fig. 4 G) when compared with nonTg WT controls. Changes in spine morphology and concomitant altered synaptic plasticity similar to AT-1 Tg mice have been observed in several animal models of neurological disorders (Auffret et al., 2009; Auerbach et al., 2011; Amini et al., 2013; Neuhofer et al., 2015). Importantly, when exposed to Dox during development to repress expression of the transgene, AT-1 Tg mice displayed neither electrophysiological nor morphological changes (unpublished data).

To better understand the mechanisms driving the observed changes in neuron structure and activity in AT-1 Tg mice, we selected target proteins known to be involved in neuronal outgrowth and synaptic plasticity, and compared expression levels in the hippocampi of Tg and WT mice (Fig. 4 H). Neurexin1, Neuroligin3, and Rap2a were selected as indicators of dendritic branching and synapse formation (Craig and Kang, 2007; Kawabe et al., 2010). AMPA2/3/4, mGluR5, synaptogyrin1, synapsin3, and Rab12 were selected

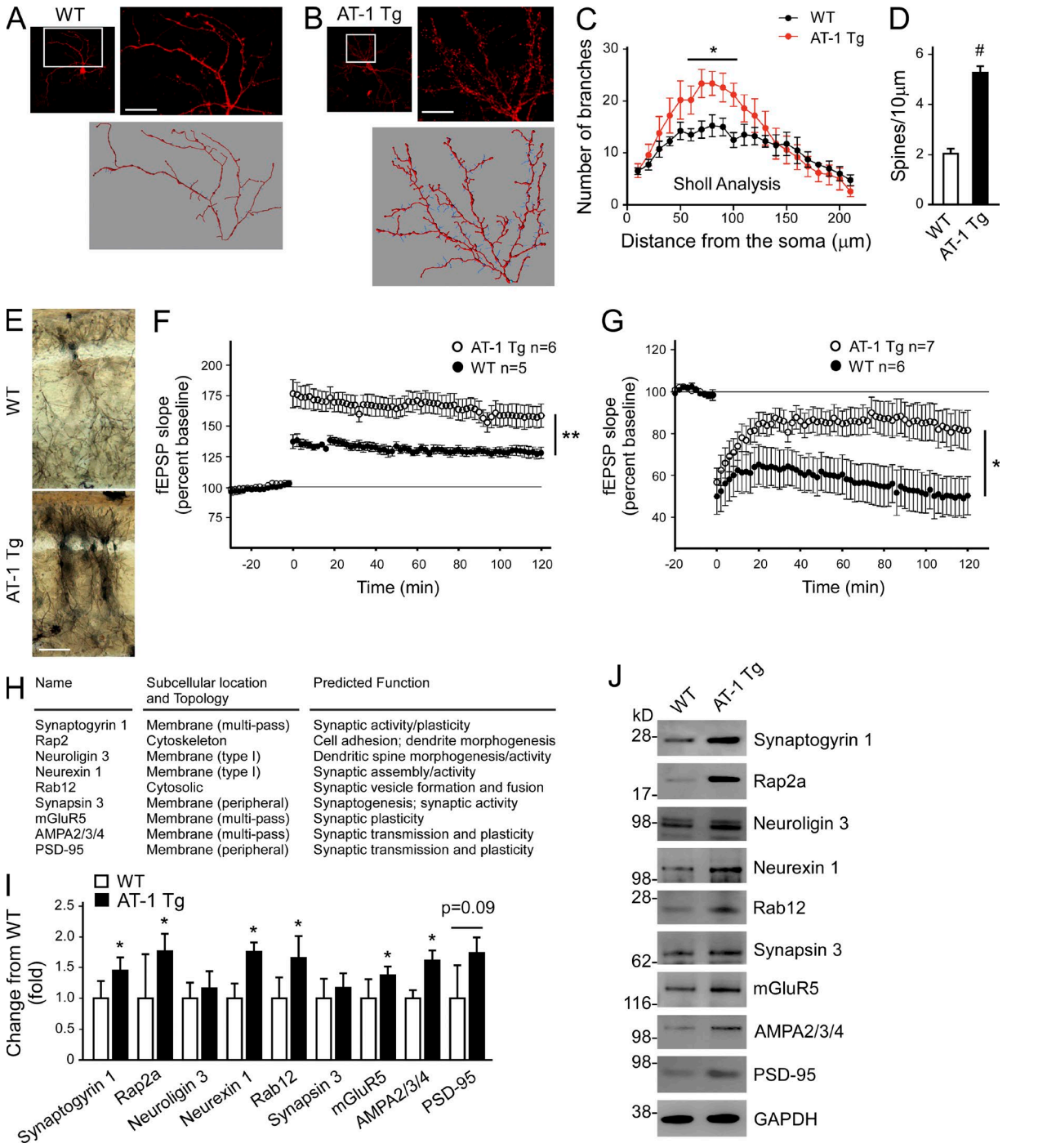

Figure 4. **AT-1 Tg animals display changes in neuronal morphology and imbalanced synaptic plasticity.** (A–D) Morphological assessment of hippocampal neurons in culture. Phalloidin staining (top) and unbiased computer-driven reconstruction (bottom) of both WT and AT-1 Tg neurons (A and B) are shown. Sholl analysis (C) and spines quantification (D) are shown. Bars, 25 μm. Number of determinations for Sholl analysis: WT, n = 4; AT-1 Tg, n = 5. Number of independent segments analyzed for spine density: WT, n = 16; AT-1 Tg, n = 36. (E) Golgi staining of the hippocampus from 6-mo-old WT and AT-1 Tg mice. Bar, 50 μm. (F) 3xTBS induced LTP in WT and AT-1 Tg mice. (G) paired pulse low-frequency facilitation LTD in WT and AT-1 Tg mice. (H–J) Western blot of selected relevant proteins. List and function of targeted proteins (H), quantification (I; n = 5), and representative Western blots (J) are shown. GAPDH served as loading control. *, $P < 0.05$; **, $P < 0.005$; #, $P < 0.0005$. Student's t test and one-way ANOVA, followed by Tukey-Kramer multiple comparisons test; for LTP and LTD, repeated measures ANOVA, followed by Bonferroni post hoc tests. Bars represent mean ± SD.

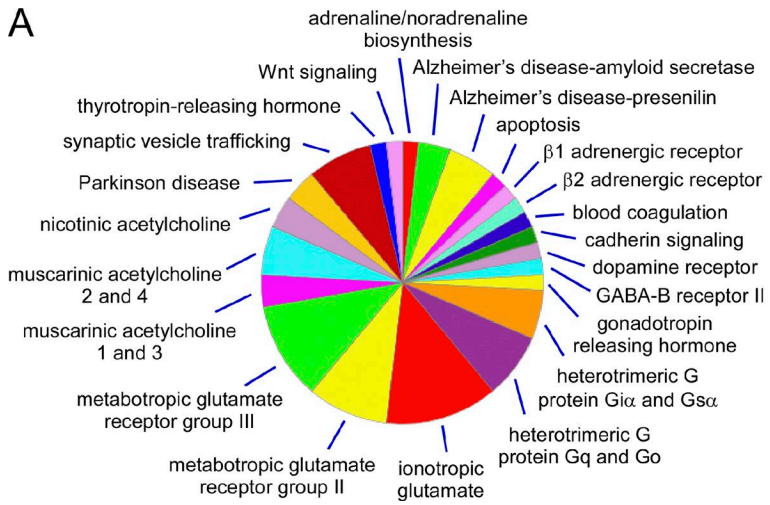

B

Cluster	Overall Function
a.	Protein synthesis and folding
b.	Lysosomal acidification membrane transporters
c.	Cell surface Na^+/K^+ transporters
d.	Synaptic activity and structure
e.	Neuronal adhesion
f.	Neurite outgrowth

Figure 5. **Analysis of the brain-specific ER acetylome in AT-1 Tg mice.** (A) PANTHER analysis of identified acetylated ER-cargo proteins. Proteins were grouped based on biological functions. (B) Clusters of highly related proteins identified by STRING analysis. Proteins were grouped based on biological function. Analysis was done in triplicate. See Table S1.

as markers of pre- and postsynaptic plasticity (Chia et al., 2013; Alvarez-Castelao and Schuman, 2015; Martenson and Tomita, 2015). We found that a majority of these proteins were significantly up-regulated in postsynaptic densities of Tg animals compared with controls (Fig. 4, I and J). Similar results were also obtained by mass spectrometry (Table S2).

AT-1 Tg animals display widespread proteomic changes

Recognized functions of Nε-lysine acetylation include regulation of expression, activity, molecular stabilization, and conformational assembly of a protein (Kouzarides, 2000). Proteomic studies have shown that a wide range of proteins undergoes Nε-lysine acetylation within the lumen of the ER; they include both ER-resident and -transiting proteins with a variety of biological functions (Choudhary et al., 2009; Pehar et al., 2012b). We have previously shown that changes in expression and activity of AT-1 have profound effects on the ER acetylation profile; specifically, increased activity leads to increased acetylation of ER cargo proteins (Jonas et al., 2010), whereas reduced activity has the opposite effect (Peng et al., 2014).

To dissect the molecular mechanisms of the AT-1 Tg phenotype, we first resolved the neuron-specific ER acetylome of the adult AT-1 Tg brain. The analysis identified 395 acetylation sites on 152 proteins (Table S1) involved in different biological pathways, as assessed by the PANTHER classification system (Fig. 5 A). STRING analysis identified six major clusters (Fig. 5 B), all highly relevant to our observed phenotype, suggesting that the increased acetylation of proteins may have consequences for neuronal outgrowth and adhesion, synaptic activity and structure, cell surface transporters, and protein synthesis.

To further elucidate the impact of increased AT-1 activity on protein expression, we conducted large-scale liquid chromatography coupled to tandem mass spectrometry (MS) analysis to identify global changes in the proteome of AT-1 Tg animals. We found that in hippocampal tissue, 476 proteins were up-regulated in Tg mice compared with CamK2 controls (Table S2). CamK2 mice were selected as the control group to correct for possible nonspecific variations in protein expression. Identified proteins were responsible for a variety of biological functions (Fig. 6 A). STRING analysis at 90% confidence revealed eight clusters that were highly correlated to the observed clusters in the acetylome data (Fig. 6 B).

When viewed globally, the acetylome (Fig. 5) and proteome (Fig. 6) data identify four major biological functions: (1) protein translation and quality control; (2) transport of synaptic vesicles, assembly of synaptic connections, and regulation of synaptic activity; (3) neuronal migration, outgrowth and adhesion; (4) mitochondria activity, specifically electron transport chain, tricarboxylate acid cycle, and acetyl-CoA metabolism. Therefore, these data suggest that the increased influx of acetyl-CoA into the ER lumen in AT-1 Tg mice affects proteins related to synaptic plasticity, neuron structure, transporter activity, and protein synthesis.

AT-1 Tg mice display increased efficiency of the secretory pathway

The proteome data (Fig. 6) indicated that 163 out of 476 proteins up-regulated in AT-1 Tg mice are either membrane or secreted proteins that are normally translated on the ER surface and inserted into the secretory pathway (Table S2). Although they are involved in different biochemical and cellular functions, STRING analysis revealed that the great majority of them are tightly related to synaptic plasticity (unpublished data), thus highlighting the significance of these proteins for our observed phenotype.

We recently reported that the ER-based acetyltransferases, ATase1 and ATase2, associate with the oligosaccharyl

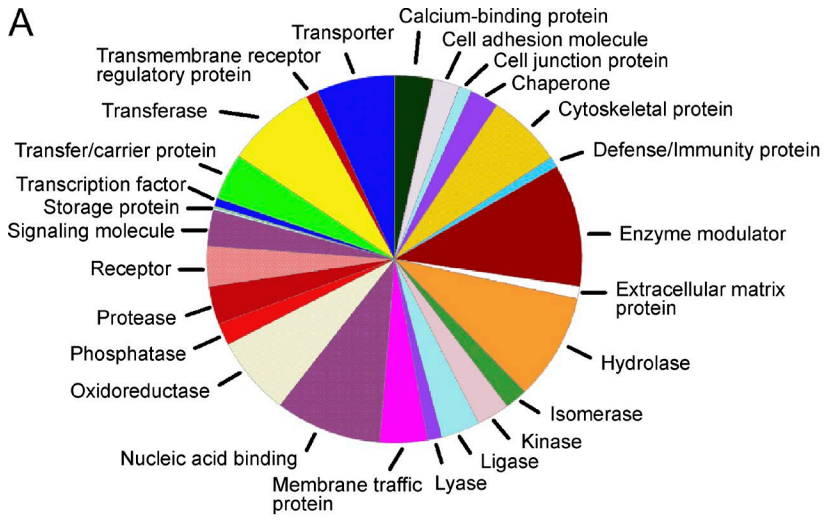

Figure 6. **AT-1 Tg animals display widespread proteomic changes.** (A) PANTHER analysis of up-regulated proteins. (B) Clusters of related proteins identified by STRING analysis at high confidence (90%). Proteins were grouped based on biological functions. Analysis was done in triplicate. See Table S2.

transferase complex to acetylate correctly folded glycoproteins (Ding et al., 2014). Studies conducted with two type I membrane glycoproteins suggest that Nε-lysine acetylation might regulate efficiency of transport along the secretory pathway (Costantini et al., 2007; Mak et al., 2014). To investigate whether increased influx of acetyl-CoA into the ER lumen can indeed cause global changes in the efficiency of transport in the secretory pathway, we used human neuroglioma (H4) cells overexpressing AT-1. Cells were labeled with azide-modified mannosamine (ManNAz), which is metabolically incorporated into sialic acid–containing glycoproteins while they traffic through the secretory pathway (Laughlin and Bertozzi, 2007). Sialic acid is the last sugar to be attached to the oligosaccharide chain; both the Golgi-membrane cytidine monophosphate-sialic acid transporter and the Golgi-resident sialyltransferase are located in the trans-Golgi (Hirschberg et al., 1998). Only nascent glycoproteins that have successfully reached the trans-Golgi can be sialylated (Hirschberg et al., 1998). Therefore, ManNAz can specifically determine efficiency of trafficking of newly synthesized glycoproteins. The results show a dramatic increase in the levels of nascent glycoproteins as a result of AT-1 overexpression (Fig. 7 A). To account for possible changes in protein translation, we also labeled cells with O-propargyl-puromycin (OPP), an alkyne analogue of puromycin that incorporates into newly translated proteins. The results revealed a significant increase in rate of protein biosynthesis (Fig. 7 B). However, normalization of ManNAz (rate of transport) and OPP (rate of biosynthesis) labeling still showed increased delivery of secretory glycoproteins to the cell surface (Fig. 7 C). Importantly, OPP incorporation does not discriminate between secretory and nonsecretory proteins, whereas ManNAz does. Therefore, we can conclude that although increased translation can partially account for the increased levels of secretory proteins in AT-1 Tg mice, increased efficiency of transport along the secretory pathway is likely to play a major role. To support the studies conducted with ManNAz, we also determined levels of cell-surface biotinylated proteins. Again, we found a significant increase in AT-1–overexpressing cells (Fig. 7 D). Using a cell-impermeable reagent to biotinylate primary amines can be used as a reliable readout of steady-state levels of cell-surface proteins. Biotin labeling does not visualize secreted proteins or proteins that localize to intracellular organelles (i.e.; Golgi apparatus, lysosomes, etc.). Therefore, in contrast to ManAz labeling, it underestimates the efficiency of the secretory pathway. However, the biotin read-out (Fig. 7 D) is consistent with the ManAz results (Fig. 7 A). Finally, to confirm the aforementioned conclusions, we also determined ManNAz incorporation in mouse embryo fibroblasts (MEFs) generated from AT-$1^{S113R/+}$ mice. AT-1_{S113R} is a mutant version of AT-1 associated with a familial form of spastic paraplegia (Lin et al., 2008) and is deficient in acetyl-CoA transport activity (Peng et al., 2014). As a result, AT-$1^{S113R/+}$ mice represent a model of AT-1 haploinsufficiency (Peng et al., 2014). As expected, we observed a significant reduction in levels of cell-surface glycoproteins in AT-$1^{S113R/+}$ MEFs (Fig. 7 E), thus supporting the conclusion that influx of acetyl-CoA into the ER lumen regulates efficiency of trafficking of secretory glycoproteins.

When taken together, the above results suggest that AT-1 Tg mice have increased delivery of ER cargo proteins to the cell surface. The same animals also have increased levels of 163 proteins that are translated on the ER and insert into the secretory pathway (Table S2). It is likely that these two findings are functionally related and that they play an important role in the observed mouse phenotype.

Increased activity of AT-1 leads to mitochondria adaption

In addition to changes in the efficiency of the secretory pathway, the proteomics results (Fig. 6 and Table S2) revealed a

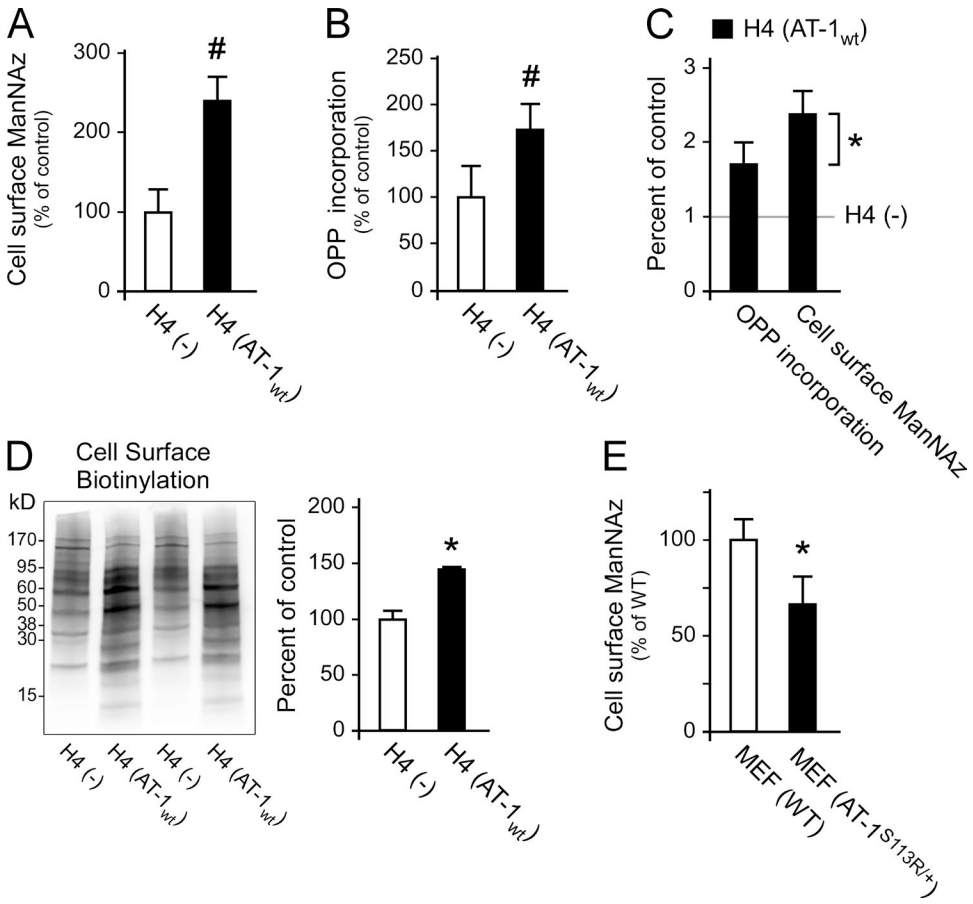

Figure 7. **AT-1 Tg mice display increased efficiency of the secretory pathway.** (A) Incorporation of ManNAz into sialic acid–containing glycoproteins to assess efficiency of trafficking of newly synthesized glycoproteins. H4(-), transfected with empty vector; H4(AT-1_{wt}), transfected with AT-1_{wt}. (H4(-), n = 8; H4(AT-1_{wt}), n = 9). (B) Incorporation of OPP to determine rate of protein biosynthesis. (H4(-), n = 21; H4(AT-1_{wt}), n = 25). (C) Normalization of ManNAz labeling per rate of OPP incorporation. (D) Western blot assessment of cell surface biotinylated proteins. Left, representative images; right, quantitation. (H4(-), n = 2; H4(AT-1_{wt}), n = 2). (E) Incorporation of ManNAz into sialic acid–containing glycoproteins to assess efficiency of trafficking of newly synthesized glycoproteins into MEFs generated from WT and AT-$1^{S113R/+}$ mice. (MEF(WT), n = 35; MEF(AT-$1^{S113R/+}$), n = 43). *, $P < 0.05$; #, $P < 0.0005$. Student's t test. Bars represent mean ± SD.

marked up-regulation of proteins related to three important mitochondrial functions: electron chain transport, tricarboxylate acid cycle, and acetyl-CoA metabolism (Fig. 8 A). It is worth remembering that the ER imports acetyl-CoA from the cytosol and that the cytosolic pool of acetyl-CoA is largely supplied by the conversion of mitochondria-derived citrate into acetyl-CoA (Pehar and Puglielli, 2013; Pietrocola et al., 2015). Given the increased influx of cytosolic acetyl-CoA into the ER lumen, caused by the overexpression of AT-1, we hypothesized that levels of cytosolic acetyl-CoA would be decreased in AT-1 Tg mice, forcing the mitochondria to compensate by generating more citrate for cytosolic conversion. To test this hypothesis, we initially determined acetyl-CoA levels in the cytosol of AT-1–overexpressing H4 cells. The results showed a significant reduction when compared with control cells (Fig. 8 B), supporting the conclusion that the increased flux into the ER lumen is able to affect the cytosolic pool of acetyl-CoA. To assess whether this conclusion could be extended to the in vivo settings, we also analyzed the cytosol recovered from total hippocampal tissue (Fig. 8 C), as well as isolated adult cortical neurons (Fig. 8 D) of AT-1 Tg mice. Again, we observed a significant reduction of acetyl-CoA levels when compared with WT mice. Importantly, two crucial proteins that allow cross-talk between mitochondria and cytosolic acetyl-CoA were also found to be up-regulated in our proteomics analysis: the mitochondrial carrier citrate transporter (Slc25a1) and Acly (Table S2). Slc25a1 is the mitochondria membrane transporter that translocates citrate to the cytosol, whereas Acly is a cytosolic-based enzyme that converts mitochondria-derived citrate into acetyl-CoA by using cytosolic CoA and ATP (Pehar and Puglielli, 2013; Pietrocola et al., 2015). Interestingly, Acss2 (also known as AceCS), which contributes to the synthesis of cytosolic acetyl-CoA through the condensa-

tion of acetate and CoA (Pehar and Puglielli, 2013; Pietrocola et al., 2015), was not found to be up-regulated (Table S2). It is worth stressing that although both Acly and Acss2 can generate acetyl-CoA, they carry out two different biochemical reactions; they also respond to different inputs and elicit different biological functions (Wellen et al., 2009; Xu et al., 2014). Therefore, our results would suggest that Acly, but not Acss2, is activated to ensure mitochondria adaptation in the AT-1 Tg mice. To investigate this further, we also determined mRNA levels of *Slc25a1*, *Acly*, and *Acss2* in the hippocampus of AT-1 Tg mice. Again, *Slc25a1* and *Acly* showed significant up-regulation, whereas *Acss2* did not (Fig. 8 E).

Collectively, the aforementioned data (Fig. 8, B–E) suggest that the increased transport of acetyl-CoA into the lumen of the ER reduces levels of cytosolic acetyl-CoA, leading to increased generation and delivery of citrate from the mitochondria, followed by increased conversion of citrate into acetyl-CoA (Fig. 8 F). Therefore, we interpret the up-regulation of mitochondria-related pathways as a compensatory mechanism (here defined as mitochondrial adaptation) to the increased expression of AT-1.

The aforementioned findings raise the question of how mitochondria can sense cytosolic levels of acetyl-CoA. A possible explanation is that changes in the cytosolic pool of acetyl-CoA cause epigenetic changes, leading to transcriptional activation of targeted mitochondria enzymes. To test this possibility, we used a MS-based strategy to assess the post-translational modification profile of histone proteins within the hippocampus of WT and AT-1 Tg animals. Previous studies have correlated acetyl-CoA availability to global epigenetic changes (Wellen et al., 2009). The MS results showed a significant increase in the acetylation of H3K27 accompanied by a significant decrease in H3K27 methylation, indicative of increased transcriptional activation in our Tg animals (Fig. 9 A and Table S3). Importantly, the MS data were confirmed by direct assessment of H3K27acetyl and H3K27trimethyl levels by immunoblotting (Fig. 9 B), suggesting that a significant portion of chromatin has "sensed" the altered levels of acetyl-CoA.

When taken together, the aforementioned results suggest that the H3K27 modification might serve as a "sensor" to rapidly respond to changes in cytosolic levels of acetyl-CoA by activating key mitochondria genes. To test this hypothesis, we conducted chromatin immunoprecipitation (ChIP) analysis and probed for *SLC25A1* and *ACLY*, which are key to the mitochondrial adaptation observed in AT-1 Tg mice (see Fig. 8 F). Again, we used *ACSS2* as negative control. Immunoprecipitation with an anti-H3K27ac antibody resolved *SLC25A1* and *ACLY*, but not *ACSS2* (Fig. 9 C). When coupled to quantitative real-time PCR (qPCR), the ChIP analysis revealed increased H3K27 acetylation of *SLC25A1* and *ACLY* in AT-1–overexpressing H4 cells (Fig. 9 D). These results correlate to the increased mRNA levels of both genes shown in Fig. 8 E. To assess whether these findings could be extended to the in vivo settings, we performed the same analysis with total hippocampal tissue (Fig. 9 E) and isolated adult cortical neurons (Fig. 9 F) of AT-1 Tg mice. Again, we found increased H3K27 acetylation of *Slc25a1* and *Acly*, when compared with WT mice.

In conclusion, these findings suggest that the enhancement in acetylation at the H3K27 site directly modifies expression of genes related to mitochondrial activity, providing a selective, targeted mitochondrial adaptation to changes in cytosolic levels of acetyl-CoA.

DISCUSSION

Here, we report that mice that overexpress human AT-1 display cognitive deficits, autistic-like social behavior, aberrations in synaptic plasticity, increased number of dendritic spines and branches, and widespread proteomic changes. We also report that AT-1 activity regulates the efficiency of the secretory pathway as well as cytosolic levels of acetyl-CoA, which in turn leads to epigenetic modulation of the histone epitope H3K27 and mitochondrial adaptation. In conclusion, our results indicate that increased neuronal expression of AT-1 can cause an autistic-like phenotype by affecting key metabolic pathways.

Nε-lysine acetylation occurs on both ER-transiting and -resident proteins with a wide array of biological functions (Choudhary et al., 2009; Pehar et al., 2012b; Fig. 5). Lysine acetylation is emerging as a novel mechanism that contributes to ER-based quality control; proteins that are properly folded are acetylated and proceed through the secretory pathway, whereas proteins that are not acetylated are retained and degraded (Costantini et al., 2007; Ding et al., 2014; Mak et al., 2014). The ER-based acetylation machinery requires the membrane transporter AT-1 (Jonas et al., 2010) and at least two acetyltransferases (Ko and Puglielli, 2009).

Heterozygous and homozygous mutations in *AT-1/SLC33A1* have been identified in patients with familial spastic paraplegia (Lin et al., 2008) and developmental delay/premature death (Huppke et al., 2012), respectively. Chromosomal duplications affecting the 3q25.31 locus harboring *AT-1/SLC33A1* have been associated with ASD and intellectual disability (Sanders et al., 2011; Prasad et al., 2012; Krumm et al., 2013). Additionally, a short chromosomal gain that covered only two genes, *AT-1/SLC33A1* and *GMPS*, was found in children with autism, seizure, abnormal electroencephalogram, and facial dysmorphism (Swisshelm, K., et al. 2014. ASHG Annual Meeting, San Diego, CA). Although not definitive, the aforementioned genetic association supports a causative role of AT-1 in ASD. Importantly, chromosomal duplications of 17p13.1 (harboring *SLC13A5*), 22q11.21 (harboring *SLC25A1*), and 17q21.2 (harboring *ACLY*) have also been associated with ASD (Sanders et al., 2011). SLC13A5 is the cell surface citrate transporter that translocates citrate from the extracellular milieu to the cytosol; SLC25A1 is the mitochondria membrane citrate transporter that translocates citrate from the mitochondria to the cytosol; and ACLY is the enzyme responsible for converting cytosolic citrate into

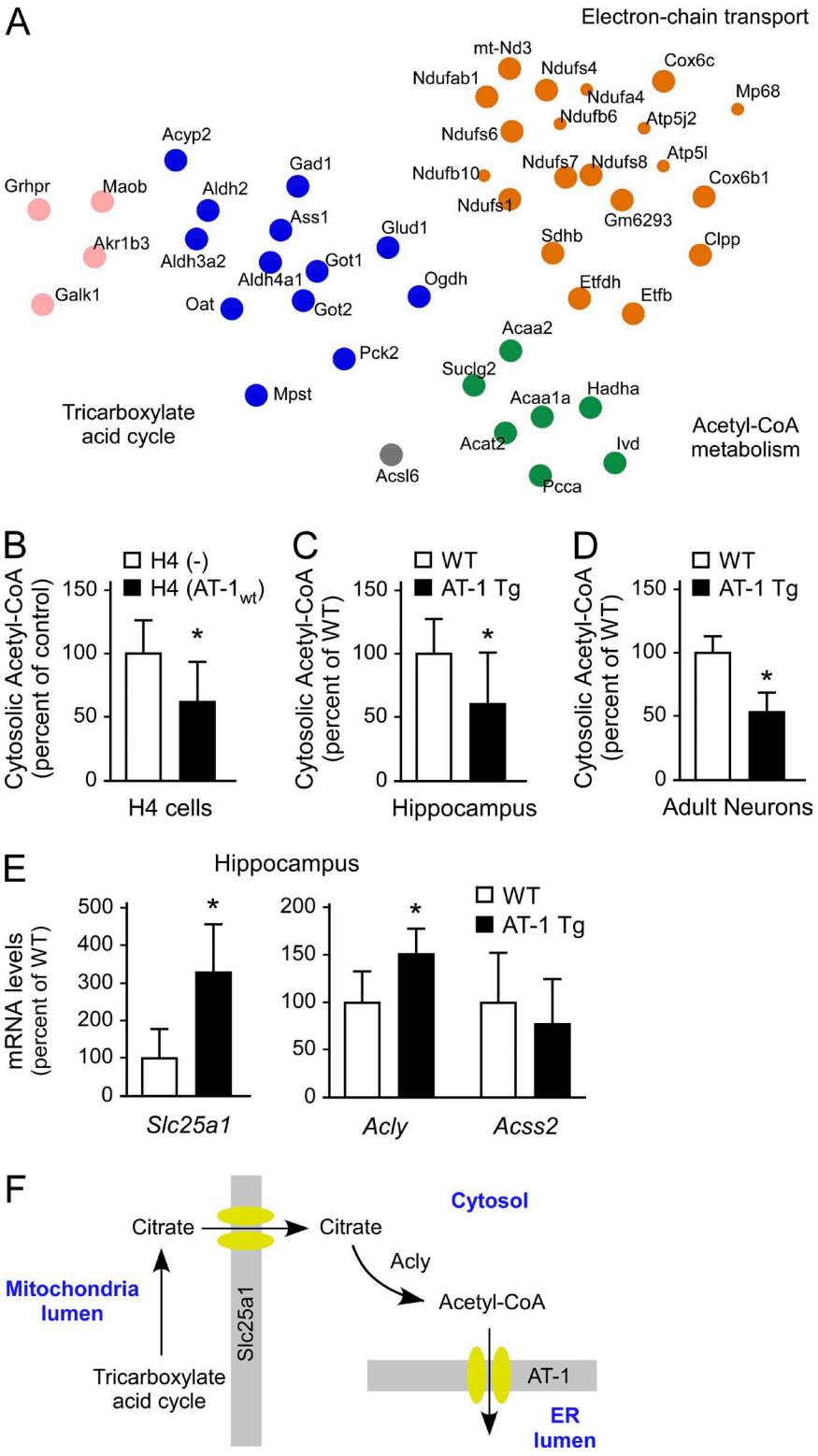

Figure 8. **Mitochondrial adaptation in AT-1 Tg mice.** (A) STRING analysis of mitochondria proteins found to be up-regulated in AT-1 Tg mice. Individual clusters are identified with different colors. Original data are shown in Table S2. (B) Cytosolic levels of acetyl-CoA in H4 cells. H4(-), control/empty vector; H4(AT-1_{WT}), overexpressing WT AT-1. Results are expressed as percent of H4(-). (H4(-), n = 10; H4 (AT-1_{WT}) n = 11). (C) Cytosolic levels of acetyl-CoA in total hippocampal tissue. (WT, n = 6; AT-1 Tg, n = 6). (D) Cytosolic levels of acetyl-CoA in isolated adult neurons. (WT, n = 3; AT-1 Tg, n = 3). (E) mRNA levels of *Slc25a1*, *Acly*, and *Acss2* in the hippocampus of AT-1 Tg mice. (WT, n = 7; AT-1 Tg, n = 6). (F) Schematic summary of results showing the mitochondrial adaptation that results from the increased influx of acetyl-CoA into the ER in AT-1 Tg mice. *, $P < 0.05$. Student's t test. Bars represent mean ± SD.

acetyl-CoA. In conclusion, these individual genetic associations affecting *SLC14A5*, *SLC25A1*, *ACLY*, and *AT-1/SLC33A1* seem to suggest a model where increased supply and movement of acetyl-CoA into the ER lumen is tightly linked to ASD. This model is supported by the phenotype of AT-1 Tg mice reported here. It is also worth mentioning that, like *SLC33A1* (Huppke et al., 2012), mutations in *SLC13A5* and *SLC25A1* have also been associated with developmen-

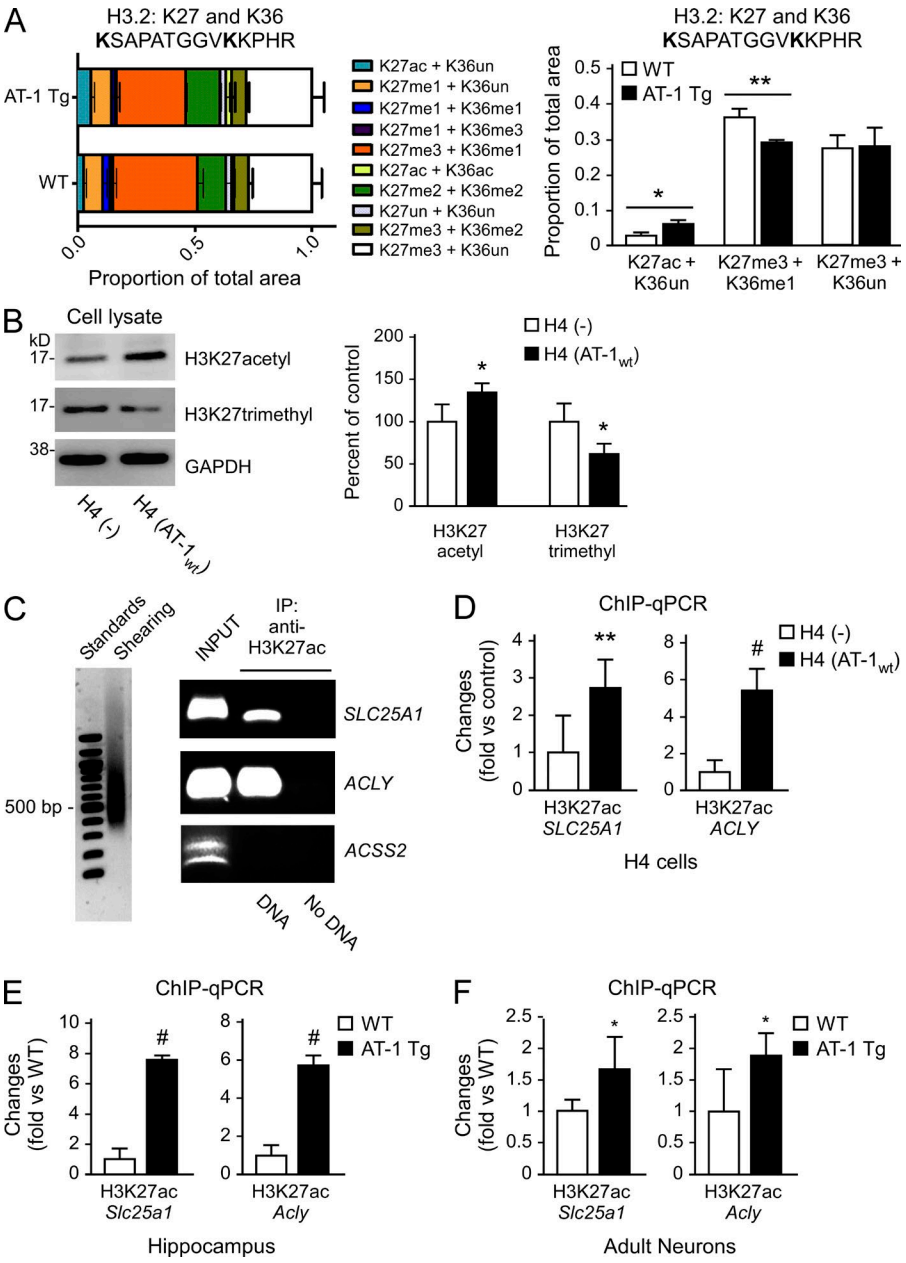

Figure 9. **The mitochondrial adaptation in AT-1 Tg mice is driven by a specific epigenetic activation.** (A) Mass spectrometry quantification of posttranslational modifications of histone proteins in the hippocampus of AT-1 Tg mice. Global changes on H3K27/K36 are shown on the left and changes in the acetylation and methylation profile of H3K27 are shown on the right (WT, $n = 3$; AT-1 Tg, $n = 3$). (B) Western blot assessment showing acetylation and methylation of H3K27 in AT-1–overexpressing H4 cells. Selected images are shown on the left panel and quantification ($n = 4$) is shown on the right. (C) ChIP analysis of *SLC33A1*, *ACLY*, and *ACSS2* after immunoprecipitation (IP) with an anti-H3K27ac antibody. IP was done in H4 cells. (left) Sheared DNA; (right) ChIP-amplification. Analysis was performed in quadruplicate. (D) ChIP-qPCR showing H3K27 acetylation of *SLC25A1* and *ACLY* in H4 cells. Results are expressed as fold of H4 (-) (H4(-), $n = 5$; H4($AT\text{-}1_{WT}$), $n = 5$). (E) ChIP-qPCR showing H3K27 acetylation of *Slc25a1* and *Acly* in total hippocampal tissue. Results are expressed as fold of WT (WT, $n = 3$; AT-1 Tg, $n = 3$). (F) ChIP-qPCR showing H3K27 acetylation of *Slc25a1* and *Acly* in isolated adult neurons. Results are expressed as fold of WT (WT, $n = 3$; AT-1 Tg, $n = 3$). IP in D–F was performed with an anti-H3K27ac antibody. *, $P < 0.05$; **, $P < 0.005$; #, $P < 0.0005$. Student's *t* test and one-way ANOVA followed by Tukey-Kramer multiple comparisons test. Bars represent mean ± SD.

tal delay of the brain (Thevenon et al., 2014; Hardies et al., 2015; Prasun et al., 2015). In addition, single variants on several other genes that are directly or indirectly related to the citrate-acetyl-CoA metabolic pathway have been identified in ASD cohorts. Some of them have also been associated with developmental delay and epileptic encephalopathy. These include *SLC16A3*, *SLC16A7*, *SLCA1*, *SLCA2*, *SLC25A12*, *SLC25A14*, *SLC25A24*, and *SLC25A27* (Sanders et al., 2011).

The molecular basis behind the observed AT-1 Tg phenotype involves increased transport of acetyl-CoA into the lumen of the ER, likely causing changes in the ER acetylome, as well as in the efficiency of the secretory pathway. The ability of Nε-lysine acetylation to regulate activity and/or levels of modified proteins is well documented (Kouzarides, 2000; Pehar and Puglielli, 2013; Pietrocola et al., 2015). Both the acetylome (Fig. 5) and the proteome (Fig. 6) identified a large set of proteins that are implicated in cellular functions that could immediately explain the Tg mouse phenotype, specifically: neuronal migration and adhesion, neurite outgrowth, transport of synaptic vesicles, assembly of synaptic connections, and regulation of synaptic activity. Therefore, it is conceivable to assume that the increased influx of acetyl-CoA, and consequent changes in the ER acetylome and in the efficiency of the secretory pathway, is the primary cause of ASD-like phenotype.

The characterization of the AT-1 Tg phenotype also revealed that the animals display decreased levels of cyto-

solic acetyl-CoA and, as a result, mitochondrial adaptation. This adaptive mechanism appears to be driven by epigenetic changes on H3K27. Importantly, we did not detect widespread epigenetic changes (Table S3). This is likely a result of the compensatory activity of Acly; indeed, silencing of *ACLY* in mammalian cells causes global changes in histone acetylation (Wellen et al., 2009). Whether the mitochondria adaptation participates in the observed phenotype remains to be fully determined. The fact that genes, such as *SLC13A5* and *ACLY*, which can alter cytosolic levels of acetyl-CoA without affecting mitochondria activity directly, might be linked to ASD (discussed above) would suggest that mitochondria have limited impact. However, genes such as *SLC25A12* and *SLC25A1*, which immediately influence acetyl-CoA production or delivery from the mitochondria, have also been linked to ASD. Therefore, the role of mitochondria might be more complex than expected. It is also possible that crosstalk exists between mitochondria, cytosol, and ER so that either increased supply (from mitochondria and/or cytosol) or movement of acetyl-CoA into the ER lumen causes ASD. In conclusion, the specific role of the mitochondria citrate pathway and of the cytosolic citrate/acetyl-CoA pools in ASD remains to be fully dissected.

Although increased efficiency of the secretory pathway seems to be logically connected to increased expression of proteins related to synaptic plasticity and learning and memory formation, a majority of proteins identified by mass spectrometry do not insert into the secretory pathway. However, the dramatic increase in dendritic spine and branch formation observed in our animals would require targeted (and secondary) up-regulation of cytosolic and nuclear proteins related to neurite outgrowth. Establishing synaptic densities would also require the activation of cytosolic scaffolding and adaptor proteins that support the structural integrity of the synapse as well as regulate signal transduction pathways. Indeed, our proteomic assessment found significant increase of cytosolic proteins that are involved in different aspects of the aforementioned biological pathways.

In conclusion, our studies have revealed that both decreased (Peng et al., 2014) and increased (present study) AT-1 activity affect neuronal biology. In particular, the data shown here have linked increased AT-1 activity to ASD, and elucidated a novel aspect of acetyl-CoA metabolism that affects learning and memory, synaptic plasticity, protein expression, mitochondrial activity, and epigenetics. Further studies are necessary to determine whether changes in AT-1 activity at various points in the lifespan of the mouse will induce significant changes in neuronal morphology and behavior.

MATERIALS AND METHODS

Generation of AT-1 Tg mice

cDNA encoding human AT-1 was isolated by BamHI and EcoRV digestion from Topo-AT-1 constructs and subcloned into pTRE-Tight vector (Takara Bio Inc.). TRE-AT-1 Tg lines were generated by injection of linearized pTRE-Tight vector (Takara Bio Inc.) containing AT-1 cDNA into the pronucleus of fertilized eggs from FVB mice. Monogenic pTRE-AT-1 mice were backcrossed to WT C57BL/6 mice for five generations, and then bred to CamK2a-tTA mice (B6.Cg-Tg(Camk2a-tTA)1Mmay/DboJ; The Jackson Laboratory), generating nonTg WT, Camk2a-tTA monogenic, TRE-AT-1 monogenic, and CamK2a-tTA;TRE-AT-1 (referred to as AT-1 Tg) mice. Genotyping from tail DNA was performed using the following primers: AT-1 forward (5′-AATCTGGGAAAC TGGCCTTCT-3′), AT-1 reverse (5′-TATTACCGCCTT TGAGTGAGCTGA-3′), Camk2a-tTA forward (5′-CGC TGTGGGGCATTTTACTTTAG-3′), and Camk2a-tTA reverse (5′-CATGTCCAGATCGAAATCGTC-3′).

Animal experiments were performed in accordance with the National Institutes of Health Guide for the Care and Use of Laboratory Animals, and were approved by the Institutional Animal Care and Use Committee of the University of Wisconsin-Madison and the Madison Veterans Administration Hospital. Unless specified, WT littermates were used as control throughout our study.

Cell cultures

Mouse embryonic fibroblasts (MEFs) from WT and AT-$1^{S113R/+}$ mice were previously described (Peng et al., 2014), and AT-1–overexpressing H4 (human neuroglioma) cells were previously described (Jonas et al., 2010; Pehar et al., 2012b). MEFs and H4 cells were maintained in DMEM supplemented with 10% FBS and 1% Penicillin/Streptomycin/Glutamine solution (Mediatech, Inc). G418 was used as selection marker in $H4_{AT\text{-}1}$ cells (Jonas et al., 2010; Pehar et al., 2012b).

Adult neurons were isolated as previously described (Cahoy et al., 2008). In brief, mouse brains were quickly removed and digested with Neural Tissue Dissociation kit (Miltenyi Biotec) and gentleMACS Dissociators (Miltenyi Biotec). After enzymatic and mechanical dissociation, the cell suspension was passed through a 40-µm cell strainer and washed with HBSS. The pellets were spun down at 300 *g* for 10 min and resuspended with buffer from a Neuron Isolation kit (Miltenyi Biotec). Non-neuron cells were removed by using Non-Neuron Cells Biotin-Antibody Cocktail (Miltenyi Biotec), followed by Anti-Biotin MicroBeads (Miltenyi Biotec). After magnetic separation with QuadroMACS Separator (Miltenyi Biotec), the neuronal cells were collected as the unlabeled fraction from the flow-through part.

Primary neuronal cultures were generated from E17-E18 mice. The isolated hippocampus was digested in 0.25% trypsin-EDTA (Gibco) for 15 min at 37°C, followed by trituration into a single-cell suspension with fire-polished glass pipettes. The dissociated cells were resuspended in the plating medium (Dulbecco's modified Eagle's medium with 10% FBS). The cells were plated onto coverslips precoated with poly-D-lysine (100 µg/ml; Sigma-Aldrich) at a density of 150 cells/mm^2. 4 h after plating, media was changed to a serum-free neurobasal medium supplemented with 2% B27 (Gibco) and 0.5 mM GlutaMAX (Invitrogen). Media was

changed every 3 d. Cultures were maintained in 37°C and 5% CO_2 incubator for up to 21 d. For immunocytofluorescence analysis, cultures were fixed with 4% paraformaldehyde and immunostained with NeuN antibody (clone A60; 1:100; EMD Millipore) and tetramethyl rhodamine isothiocyanate (TRITC)-labeled phalloidin (0.5 µg/ml; Sigma-Aldrich). Nuclei were counterstained with DAPI.

Behavioral analysis

All behavioral tests were conducted and analyzed by an experimenter blind to the genotype of the mice. Unless indicated, mice were approximately 6-mo-old when tested.

MWM. The test consisted of eight blocks of testing over 4 d, followed by a probe trial. The first day, mice were briefly exposed to the pool to test swimming capabilities. Each mouse received two blocks of testing per day for 4 d, and each block was comprised of four sequential trials, for a total of 32 training trials. Each trial, the mouse was placed into the pool at a different start location and allowed to swim until it either located the platform, or reached the end of the 60-s trial. Behavior was monitored by an overhead camera and Noldus Ethovision software. If the mouse did not locate the platform within the 60-s time limit, it was gently placed on the platform and allowed to rest and look around for a few seconds before beginning the next trial. On the final day of testing, after completing the eighth block of testing, mice were exposed to the pool for a probe trial. For this trial, the platform was removed, and swimming behavior was monitored for 60 s.

NOR. Each mouse received five sequential 6-min trials, with a 3-min inter-trial interval. The first trial allowed the mouse to acclimate to the empty arena, with no objects presented. Trials two to four were training trials with four objects presented within the arena. For the testing trial, one randomly selected object was removed and replaced with a novel object. This trial was videotaped and subsequently analyzed by a trained observer blind to both mouse condition and the identity of the novel object. Time spent investigating all objects was used as total investigative time; the time spent exploring each object was expressed as percentage total investigative time. All objects used were pretested to guarantee no innate preference, and the novel object was rotated through a pool of these objects.

FC. Mice were tested in the delay FC paradigm to assess contextual memory formation. On day 1, mice were exposed to a 6-min training protocol, which consisted of two 30-s pairings of 87 dB white noise and a 1.5-s 0.7 mA shock, with an inter-trial interval of 2 min. On day 2, 22 h after exposure to the training protocol, mice were tested for conditioning to context. Mice were placed back in the chambers in which they originally received the shock for 5 min, but no stimuli (noise or shock) were presented. Percent freezing during each portion of the FC paradigm was calculated by the FreezeFrame 3 software (Coulbourn) using video feed and a motion index.

Marble burying. The marble burying paradigm was used to assess repetitive behaviors. Each mouse was placed into a clean cage with extra bedding and 20 black marbles arranged in a grid pattern. After 30 min of exploration in the cage, the number of marbles completely buried in the bedding and the number of marbles buried >50% were counted.

Social interaction. The social interaction test was used to assess autistic-like social behaviors in the AT-1 Tg mouse model. The test was conducted in a three-chambered arena with a central compartment and two side compartments. The test consisted of three trials, each 10 min in length, run consecutively. In the first trial, the experimental mouse was exposed to an empty arena and allowed to explore freely. In the second trial, a male juvenile mouse was placed in a mesh cup in one side chamber of the box and an identical empty mesh cup was placed in the opposite side chamber of the box to provide a neutral object control. The mesh cup allowed for visual and scent cues, but prevented aggressive behavior between the mice. During the third trial, the juvenile stimulus mouse from trial two was kept in the test arena, and a novel juvenile male mouse was placed in a cup in the opposite chamber. All trials were videotaped and used for subsequent analysis. Investigation time was scored by a trained observer blind to genotype.

Assessment of neuronal morphology

Confocal images of cultured neurons were uploaded and analyzed in Imaris 8 (Oxford Instruments) using FilamentTracer module. Filaments and spines were traced, segmented, and assigned using semiautomatic and manual detection methods. Two-dimensional rendering of cells was created based on FilamentTracer analysis in Imaris, using cylinder display. Data were extracted into Prism 6 (Graphpad), and statistical significance was determined by performing Student's *t* test and ANOVA.

Golgi staining

Brains were harvested from 6-mo-old mice and Golgi stained using the FD Neurotech Golgi kit. In brief, brains were immersed in equal parts solution A and solution B and allowed to sit for 2 wk. Brains were moved into solution C for 72 h, and then sliced to 100 µM thickness using a sliding microtome.

Electrophysiology

Extracellular recordings of field excitatory postsynaptic potentials (fEPSP), were measured from acute hippocampal slices (400 µm) prepared as previously described (Pehar et al., 2010). In brief, enameled bipolar platinum–tungsten-stimulating electrodes were placed along Schaffer collaterals, and fEPSPs were recorded with ACSF-filled recording electrodes (2–4 MOhm) from area CA1 stratum radiatum. Baseline responses were set to an intensity that evoked an fEPSP with a slope of 50% that of the maximum evoked response. For LTP, 3x theta burst (3xTBS) consisted of a total of three trains of 10 bursts (each burst consisting of four stimulations at a

frequency of 100 Hz) with an interburst interval of 200 ms. For LTD, paired pulse low frequency stimulation consisted of 900 pairs of stimuli with a 50-ms paired pulse interval. Input/output curves were performed before and at the end of LTD recordings to ensure slice health. Data were analyzed by two-way ANOVA (treatment and time) with repeated measures (mixed model) and Bonferroni post-hoc tests.

Postsynaptic densities (PSDs)

Hippocampal tissue was homogenized in Tris-acetate buffer (50 mM, pH 7.4) containing 100 µM EGTA, 0.32 M sucrose, and protease and phosphatase inhibitors. Homogenate was centrifuged at 1,000 *g* for 10 min. Supernatants were then centrifuged at 14,000 *g* for 20 min, and the resulting pellet was defined as the crude synaptosomal fraction. Synaptosomes were resuspended in Tris-acetate buffer. To purify the PSDs, the synaptosomal fraction was diluted with 20 mM Tris-HCl, pH 6.0, and 0.1 mM $CaCl_2$ containing 1% Triton X-100, mixed for 20 min at 4°C on a plate rocker, and then centrifuged at 25 p.s.i. for 20 min using an air-driven ultracentrifuge (Airfuge; Beckman Coulter). The pellet was resuspended in 20 mM Tris-HCl, pH 8.0, and 0.1 mM $CaCl_2$ containing 1% Triton X-100. Samples were mixed again for 20 min at 4°C on the plate rocker, and then centrifuged on the Airfuge (25 p.s.i.) for 20 min. The insoluble pellet containing the PSD fraction was suspended in Tris-acetate buffer (50 mM, pH 7.4, 100 µM EGTA, and 0.32 M sucrose and proteases inhibitors) and stored at −80°C until use.

Immunoblotting

Western blotting was performed on a 4–12% Bis-Tris SDS-PAGE system (NuPAGE; Invitrogen) as previously described (Costantini et al., 2006; Pehar et al., 2010; Peng et al., 2014). The following primary antibodies were used in this study: Neurexin 1 (1:1,000; Thermo Fisher Scientific; #18730) Neuroligin 3 (1:1,000; Thermo Fisher Scientific; #18849); Rap2a (1:1,000; Thermo Fisher Scientific; #23298); Synapsin 3 (1:1,000; Thermo Fisher Scientific; #25658); AMPA2/3/4 (1:1,000; Cell Signaling Technologies; #2460), mGluR5 (1:3,000; EMD Millipore; #76316); Gapdh (1:5,000; EMD Millipore; #2302); Synaptogyrin 1 (1:1,000; Abcam; #113886); Rab12 (1:1,000; Abcam; #170046); Psd-95 (1:1,000; Cell Signaling Technologies; #2507); S100 (1:1,000; Abcam; #4066); Iba1 (1:1,000; Wako; #016-20001); βIII Tubulin (1:1,000; Abcam; #18207); L1CAM (1:1,000; Abcam; #24345); NFL160 (1:5,000; Abcam; #9034); H3K27ac (1:1,000; Active Motif; #39134); and H3K27met (1:1,000; Active Motif; #39157). HRP-conjugated anti–mouse or anti–rabbit secondary antibodies were used for chemiluminescent detection (ImageQuant LAS4000; GE Healthcare); goat anti–rabbit Alexa Fluor 680–conjugated or anti–mouse Alexa Fluor 800–conjugated secondary antibodies were used for infrared imaging (LICOR Odyssey Infrared Imaging System; LI-COR Biosciences).

Proteomics studies and mass spectrometry

ER acetylome. The neuron-specific acetylome was determined as previously described (Pehar et al., 2012b). In brief, adult neurons were isolated with the gentle MACS Dissociator (Miltenyi Biotec). Proteins were digested with trypsin before high-resolution high-accuracy LC-MS/MS analysis at the Mass Spectrometry facility at the University of Wisconsin-Madison. Peptides and proteins were identified with the Mascot search engine (Matrix Science) via automated database searching of all tandem mass spectra. The output of the MS analysis was further processed to select proteins that insert into the secretory pathway.

Proteomics. Hippocampi of three pairs of Tg and control mice were dissected and two hippocampi from the same mouse were placed into the same 1.5-ml tube and stored in –80°C until homogenization. A 200 µl aliquot of lysis buffer (8 M urea, 100 mM Tris-HCl, and protease inhibitor cocktail) was added to each tube, the bottom of which was immersed in the ice bath. Next, tissues were immediately sonicated by Sonic Dismembrator (Model 120; Thermo Fisher Scientific) at 120 W output with three bursts that each lasted 45 s each. Tissues were allowed to cool on the ice bath for 30 s after each burst. The protein concentration was determined by 660 nm protein assay and 10 µg protein of each sample was used for tryptic digestion.

The protein of each sample was denatured with 8 µl of 8 M urea that was diluted by 50 mM ammonium bicarbonate buffer and reduced by 1 µl of 0.50 M DTT by incubation at 37°C for 1 h. After incubation, the reduced sample was alkylated by 2.7 µl of 0.55 M IAA and kept in the dark for 15 min. 1 µl of 0.50 M DTT was applied to quench the IAA alkylating reaction for 10 min. 70 µl of 50 mM ammonium bicarbonate was used to dilute the urea to a final concentration of 1 M, and 0.5 µg trypsin was subsequently added into the solution. The protein digestion reaction was incubated for 18 h at 37°C, and subsequently quenched by 2.5 µl of 10% formic acid. The solid phase extraction of the tryptic peptides were performed by Varian 100 µl C 18 Omix Tips (Agilent). The peptides were sequentially eluted with 60 µl 50% ACN in 0.1% formic acid, dried by SpeedVac, and reconstituted with 9 µl 0.1% formic acid. 1 µl 1 µM enolase digestion standards were spiked into each sample as internal standards.

Online reversed phase liquid chromatography separation of the tryptic peptides was performed on a nanoAcquity UPLC (Waters Corp.), and subsequently analyzed with Q Exactive quadrupole orbitrap mass spectrometer (Thermo Fisher Scientific). The chromatographic separation was performed by mobile phase A that consisted of 0.1% formic acid in water and mobile phase B with 0.1% formic acid in ACN. 1 µl of each sample was injected onto a custom-packed column that was made by silica tubing (360 µm o.d., 75 µm i.d.) with emitter tips pulled by a laser puller. The column was packed with Waters 150 Å, 1.7 µm, BEH C18 material. The LC gradient started with 5% B and increased to 30% B over 120 min at a flow rate

of 350 nl/min. Ions were generated under positive electrospray ionization (ESI) at 2.8 KV capillary voltage; 275°C capillary temperature; 30% collision energy via high-energy collision dissociation (HCD). MS1 scans were acquired over *m/z* 200–2,000 at 70 k resolution and data-dependent tandem MS scan were acquired via selection of the top 10 most abundant precursor ions by HCD fragmentation with an isolation window of *m/z* 2.0 at a resolution of 17,500. Other parameters include: automatic gain control 1×10^{-5}; maximum ion injection time, 100 ms; dynamic exclusion enabled with unassigned, +1, and greater than +8 charges ignored for MS/MS selection. Each sample was analyzed as technical triplicates.

Tryptic peptide identification was performed via Proteome Discoverer 1.4 (Thermo Fisher Scientific). FASTA file was downloaded from Uniprot's reference database of *Mus musculus* (release 2014_08) with manually added yeast enolase fasta file (SwissProt P00924). Other parameters include: allowed missed cleavage, 1; enzyme, trypsin; fixed modification, carbamidomethylation of cysteine (+57.0215 D); variable modification, oxidation of methionine (+15.9949 D); peptide mass tolerance, 10 ppm; fragment mass tolerance, 0.1 D. q value was set to achieve 1% false discovery rate via Percolator to verify the identified peptides, and the results were filtered by high confidence peptide identification. For label-free quantification of acquired data, SIEVE (Version 2.1; Thermo Fisher Scientific) was applied. The following parameters were used in the peak alignment and frame generation: m/z min = 300; m/z max = 1,500; frame time width = 6.0 min; frame m/z width = 0.02 D; retention time start = 15 min; retention time stop = 90 min; and peak intensity threshold = 10,000. Alignment was validated using the spiked enolase tryptic peptides with accurate m/z and retention time. Proteins with $P < 0.05$ were selected.

Histone extraction and LC–MS/MS analysis. Quantification of histone posttranslational modifications was performed as recently described (Krautkramer et al., 2015). Hippocampi were dounced in ice-cold nuclear isolation buffer (10 mM Tris-HCl, 10 mM NaCl, 3 mM $MgCl_2$, and 0.15% NP-40), and nuclei were pelleted by centrifugation. Histones were acid extracted from nuclei, derivatized with propionic anhydride, and trypsinized as previously described (Lin and Garcia, 2012). Histone peptides were injected onto a Dionex Ultimate3000 nanoflow HPLC with a Waters NanoEase C18 column (100 µm × 15 cm, 3 µm) coupled to a Thermo Fisher Scientific Q-Exactive mass spectrometer at 700 nl/min using a 2–35% gradient of acetonitrile. Histone modifications were identified and quantified using the MaxQuant (v 1.4.1.2). Spectra were searched against the human SwissProt database using a 20 ppm mass tolerance for the first search and a 4.5 ppm mass tolerance for the main search. The enzyme was specified as ArgC with zero missed cleavages. Variable modifications were set as follows: acetyl(K), butyryl(K), dimethyl(K), propionlyl(K), trimethyl(K), and propionyl(peptide N terminus). A reverse decoy database was generating within MaxQuant, and the false discovery rate was set to <0.01 for peptide spectrum matches, proteins, and modification sites.

Changes in protein expression as identified by mass spectrometry were further analyzed using the Protein ANalysis THrough Evolutionary Relationship (PANTHER) gene list analysis (Mi et al., 2013) and STRING 10 software (Szklarczyk et al., 2015) to highlight protein–protein interactions.

Acetyl-CoA determinations

Cytosol was isolated from total hippocampal tissue, isolated adult cortical neurons, and H4 cells using differential centrifugation as previously described (Ko and Puglielli, 2007; Pehar et al., 2014). Acetyl-CoA was measured using the PicoProbe kit (Abcam).

Trafficking of secretory proteins

Nascent glycoproteins were labeled using Click-It ManNAz (Life Technologies) and visualized using the Click-It Cell Reaction kit (Life Technologies). Biotinylated cell surface proteins were isolated using the Cell Surface Protein Isolation kit (Thermo Fisher Scientific) and visualized by Western blot with Streptavidin-HRP (1:10,000). Rate of protein biosynthesis was assessed using the Click-It Plus OPP Alexa Fluor 488 Protein Synthesis Assay kit (Life Technologies).

ChIP analysis

Control and AT-1–overexpressing H4 cells were cultured in complete medium in 150-mm Petri dishes until ∼70% confluent. The cells were then fixed by the addition of 280 µl of 37% formaldehyde (Sigma-Aldrich) to 10 ml of culture medium for 10 min at 37°C, harvested, and processed for ChIP using a commercially available kit (Active Motif). H3K27-DNA immune complexes were precipitated with a polyclonal antibody against H3K27ac (Active Motif). PCR was performed using primer sets for *Acly*, *Slc25a1*, and *Acss2* centered on the first exon region. Primer sets used were as follows: *Acly*: 5′-GCTTAGCCTGTGAGCTGAT-3′ (Sense), 5′-AGGTGG TGCAGATGTACTTG-3′ (AntiSense); *Slc25a1*: 5′-GAA TGGGTCGTGGTCTCAGTAG-3′ (Sense), 5′-CTGCTA GGATTGCCTTCCC-3′ (AntiSense); *Acss2*: 5′-AAGAGC GGCAGTGGAAG-3′ (Sense), 5′-TTCGATCCAGCACGT TGTAG-3′ (AntiSense). No antibody and normal IgG served as internal negative controls.

Real-time PCR

Real-time PCR was performed using the Roche 480 lightcycler and Sybr Green Real Time PCR Master Mix (Life Technologies). The cycling parameters were: 95°C, 10 s; 52°C, 20 s; and 72°C, 30 s, for a maximum of 45 cycles. Controls without reverse transcription were included in each assay. PCR primers specific to each gene were: *Slc25a1* and *Acly* (Bio-Rad Laboratories; Prime PCR assay); *Acss2*: 5′-AAG AGCGGCAGTGGAAG-3′ (sense), 5′-TTCGATCCAGCA CGTTGTAG-3′ (antisense); *Gapdh*: 5′-ACCACAGTCCAT GCCATCAC-3′ (sense), 5′-TCCACCACCCTGTTGCTG

TA-3′ (antisense). Expression levels were normalized against *Gapdh* levels and are expressed as percent of control.

Statistical analysis

Data analysis was performed using InStat 3.06 statistical software (GraphPad). Data are expressed as mean ± SD. Unless otherwise specified, comparison of the means was performed using Student's *t* test or one-way ANOVA, followed by Tukey-Kramer multiple comparisons test. Differences were declared statistically significant if $P < 0.05$. Unless otherwise specified, throughout the paper the following statistical significance is used: *, $P < 0.05$; **, $P < 0.005$; #, $P < 0.0005$.

Online supplemental material

Table S1 lists all acetylated peptides identified in the adult brain of AT-1 Tg mice. Table S2 provides the entire list of proteins identified by MS in the brain of WT and AT-1 Tg mice. Table S3 lists all posttranslational modifications of histone proteins identified in WT and AT-1 Tg mice. Online supplemental material is available at http://www.jem.org/cgi/content/full/jem.20151776/DC1.

ACKNOWLEDGMENTS

We thank Dr. Qiang Chang and Dr. Albee Messing for critical reading of an early version of this manuscript.

This work was supported by a VA Merit Award (BX001638), National Institutes of Health grants (NS094154, GM065386, DK071801, and S10RR029531), and a core grant to the Waisman Center from National Institute of Child Health and Human Development (P30 HD03352). E.R. Chapman is an Investigator of the Howard Hughes Medical Institute. R. Hullinger was supported by a National Science Foundation Graduate Research Fellowship.

The authors declare no competing financial interests.

Author contributions: R. Hullinger, M. Li, J. Wang, Y. Peng, E. Bomba-Warczak, J.A. Dowell, H.A. Mitchell, J.M. Denu, L. Li, and L. Puglielli conceived and designed experiments. R. Hullinger, M. Li, J. Wang, Y. Peng, E. Bomba-Warczak, J.A. Dowell, and H.A. Mitchell performed experiments and analyzed data. C. Burger, E.R. Chapman, J.M. Denu, L. Li, and L. Puglielli analyzed data. R. Hullinger and L. Puglielli wrote the paper. All authors contributed to writing and revision of the paper.

Submitted: 11 November 2015
Accepted: 15 April 2016

REFERENCES

Alvarez-Castelao, B., and E.M. Schuman. 2015. The regulation of synaptic protein turnover. *J. Biol. Chem.* 290:28623–28630. http://dx.doi.org/10.1074/jbc.R115.657130

Amini, M., C.L. Ma, R. Farazifard, G. Zhu, Y. Zhang, J. Vanderluit, J.S. Zoltewicz, F. Hage, J.M. Savitt, D.C. Lagace, et al. 2013. Conditional disruption of calpain in the CNS alters dendrite morphology, impairs LTP, and promotes neuronal survival following injury. *J. Neurosci.* 33:5773–5784. http://dx.doi.org/10.1523/JNEUROSCI.4247-12.2013

Auerbach, B.D., E.K. Osterweil, and M.F. Bear. 2011. Mutations causing syndromic autism define an axis of synaptic pathophysiology. *Nature.* 480:63–68. http://dx.doi.org/10.1038/nature10658

Auffret, A., V. Gautheron, M. Repici, R. Kraftsik, H.T. Mount, J. Mariani, and C. Rovira. 2009. Age-dependent impairment of spine morphology and synaptic plasticity in hippocampal CA1 neurons of a presenilin 1 transgenic mouse model of Alzheimer's disease. *J. Neurosci.* 29:10144–10152. http://dx.doi.org/10.1523/JNEUROSCI.1856-09.2009

Cahoy, J.D., B. Emery, A. Kaushal, L.C. Foo, J.L. Zamanian, K.S. Christopherson, Y. Xing, J.L. Lubischer, P.A. Krieg, S.A. Krupenko, et al. 2008. A transcriptome database for astrocytes, neurons, and oligodendrocytes: a new resource for understanding brain development and function. *J. Neurosci.* 28:264–278. http://dx.doi.org/10.1523/JNEUROSCI.4178-07.2008

Chia, P.H., P. Li, and K. Shen. 2013. Cell biology in neuroscience: cellular and molecular mechanisms underlying presynapse formation. *J. Cell Biol.* 203:11–22. http://dx.doi.org/10.1083/jcb.201307020

Choudhary, C., C. Kumar, F. Gnad, M.L. Nielsen, M. Rehman, T.C. Walther, J.V. Olsen, and M. Mann. 2009. Lysine acetylation targets protein complexes and co-regulates major cellular functions. *Science.* 325:834–840. http://dx.doi.org/10.1126/science.1175371

Costantini, C., H. Scrable, and L. Puglielli. 2006. An aging pathway controls the TrkA to p75NTR receptor switch and amyloid beta-peptide generation. *EMBO J.* 25:1997–2006. http://dx.doi.org/10.1038/sj.emboj.7601062

Costantini, C., M.H. Ko, M.C. Jonas, and L. Puglielli. 2007. A reversible form of lysine acetylation in the ER and Golgi lumen controls the molecular stabilization of BACE1. *Biochem. J.* 407:383–395. http://dx.doi.org/10.1042/BJ20070040

Craig, A.M., and Y. Kang. 2007. Neurexin-neuroligin signaling in synapse development. *Curr. Opin. Neurobiol.* 17:43–52. http://dx.doi.org/10.1016/j.conb.2007.01.011

Dere, E., L. Dahm, D. Lu, K. Hammerschmidt, A. Ju, M. Tantra, A. Kästner, K. Chowdhury, and H. Ehrenreich. 2014. Heterozygous ambra1 deficiency in mice: a genetic trait with autism-like behavior restricted to the female gender. *Front. Behav. Neurosci.* 8:181. http://dx.doi.org/10.3389/fnbeh.2014.00181

Ding, Y., C.D. Dellisanti, M.H. Ko, C. Czajkowski, and L. Puglielli. 2014. The endoplasmic reticulum-based acetyltransferases, ATase1 and ATase2, associate with the oligosaccharyltransferase to acetylate correctly folded polypeptides. *J. Biol. Chem.* 289:32044–32055. http://dx.doi.org/10.1074/jbc.M114.585547

Feldman, D.E. 2009. Synaptic mechanisms for plasticity in neocortex. *Annu. Rev. Neurosci.* 32:33–55. http://dx.doi.org/10.1146/annurev.neuro.051508.135516

Gkogkas, C.G., A. Khoutorsky, I. Ran, E. Rampakakis, T. Nevarko, D.B. Weatherill, C. Vasuta, S. Yee, M. Truitt, P. Dallaire, et al. 2013. Autism-related deficits via dysregulated eIF4E-dependent translational control. *Nature.* 493:371–377. http://dx.doi.org/10.1038/nature11628

Hardies, K., C.G. de Kovel, S. Weckhuysen, B. Asselbergh, T. Geuens, T. Deconinck, A. Azmi, P. May, E. Brilstra, F. Becker, et al. autosomal recessive working group of the EuroEPINOMICS RES Consortium. 2015. Recessive mutations in SLC13A5 result in a loss of citrate transport and cause neonatal epilepsy, developmental delay and teeth hypoplasia. *Brain.* 138:3238–3250. http://dx.doi.org/10.1093/brain/awv263

Hirschberg, C.B., P.W. Robbins, and C. Abeijon. 1998. Transporters of nucleotide sugars, ATP, and nucleotide sulfate in the endoplasmic reticulum and Golgi apparatus. *Annu. Rev. Biochem.* 67:49–69. http://dx.doi.org/10.1146/annurev.biochem.67.1.49

Huganir, R.L., and R.A. Nicoll. 2013. AMPARs and synaptic plasticity: the last 25 years. *Neuron.* 80:704–717. http://dx.doi.org/10.1016/j.neuron.2013.10.025

Huppke, P., C. Brendel, V. Kalscheuer, G.C. Korenke, I. Marquardt, P. Freisinger, J. Christodoulou, M. Hillebrand, G. Pitelet, C. Wilson, et al. 2012. Mutations in SLC33A1 cause a lethal autosomal-recessive disorder with congenital cataracts, hearing loss, and low serum copper and ceruloplasmin. *Am. J. Hum. Genet.* 90:61–68. http://dx.doi.org/10.1016/j.ajhg.2011.11.030

Jonas, M.C., M. Pehar, and L. Puglielli. 2010. AT-1 is the ER membrane acetyl-CoA transporter and is essential for cell viability. *J. Cell Sci.* 123:3378–3388. http://dx.doi.org/10.1242/jcs.068841

Kawabe, H., A. Neeb, K. Dimova, S.M. Young Jr., M. Takeda, S. Katsurabayashi, M. Mitkovski, O.A. Malakhova, D.E. Zhang, M. Umikawa, et al. 2010. Regulation of Rap2A by the ubiquitin ligase Nedd4-1 controls neurite development. *Neuron*. 65:358–372. http://dx.doi.org/10.1016/j.neuron.2010.01.007

Ko, M.H., and L. Puglielli. 2007. The sterol carrier protein SCP-x/pro-SCP-2 gene has transcriptional activity and regulates the Alzheimer disease gamma-secretase. *J. Biol. Chem.* 282:19742–19752. http://dx.doi.org/10.1074/jbc.M611426200

Ko, M.H., and L. Puglielli. 2009. Two endoplasmic reticulum (ER)/ER Golgi intermediate compartment-based lysine acetyltransferases post-translationally regulate BACE1 levels. *J. Biol. Chem.* 284:2482–2492. http://dx.doi.org/10.1074/jbc.M804901200

Kouser, M., H.E. Speed, C.M. Dewey, J.M. Reimers, A.J. Widman, N. Gupta, S. Liu, T.C. Jaramillo, M. Bangash, B. Xiao, et al. 2013. Loss of predominant Shank3 isoforms results in hippocampus-dependent impairments in behavior and synaptic transmission. *J. Neurosci.* 33:18448–18468. http://dx.doi.org/10.1523/JNEUROSCI.3017-13.2013

Kouzarides, T. 2000. Acetylation: a regulatory modification to rival phosphorylation? *EMBO J.* 19:1176–1179. http://dx.doi.org/10.1093/emboj/19.6.1176

Krautkramer, K.A., L. Reiter, J.M. Denu, and J.A. Dowell. 2015. Quantification of SAHA-dependent changes in histone modifications using data-independent acquisition mass spectrometry. *J. Proteome Res.* 14:3252–3262. http://dx.doi.org/10.1021/acs.jproteome.5b00245

Krumm, N., B.J. O'Roak, E. Karakoc, K. Mohajeri, B. Nelson, L. Vives, S. Jacquemont, J. Munson, R. Bernier, and E.E. Eichler. 2013. Transmission disequilibrium of small CNVs in simplex autism. *Am. J. Hum. Genet.* 93:595–606. http://dx.doi.org/10.1016/j.ajhg.2013.07.024

Laughlin, S.T., and C.R. Bertozzi. 2007. Metabolic labeling of glycans with azido sugars and subsequent glycan-profiling and visualization via Staudinger ligation. *Nat. Protoc.* 2:2930–2944. http://dx.doi.org/10.1038/nprot.2007.422

Lin, S., and B.A. Garcia. 2012. Examining histone posttranslational modification patterns by high-resolution mass spectrometry. *Methods Enzymol.* 512:3–28. http://dx.doi.org/10.1016/B978-0-12-391940-3.00001-9

Lin, P., J. Li, Q. Liu, F. Mao, J. Li, R. Qiu, H. Hu, Y. Song, Y. Yang, G. Gao, et al. 2008. A missense mutation in SLC33A1, which encodes the acetyl-CoA transporter, causes autosomal-dominant spastic paraplegia (SPG42). *Am. J. Hum. Genet.* 83:752–759. http://dx.doi.org/10.1016/j.ajhg.2008.11.003

Lugo, J.N., G.D. Smith, E.P. Arbuckle, J. White, A.J. Holley, C.M. Floruta, N. Ahmed, M.C. Gomez, and O. Okonkwo. 2014. Deletion of PTEN produces autism-like behavioral deficits and alterations in synaptic proteins. *Front. Mol. Neurosci.* 7:27. http://dx.doi.org/10.3389/fnmol.2014.00027

Mak, A.B., M. Pehar, A.M. Nixon, R.A. Williams, A.C. Uetrecht, L. Puglielli, and J. Moffat. 2014. Post-translational regulation of CD133 by ATase1/ATase2-mediated lysine acetylation. *J. Mol. Biol.* 426:2175–2182. http://dx.doi.org/10.1016/j.jmb.2014.02.012

Martenson, J.S., and S. Tomita. 2015. Synaptic localization of neurotransmitter receptors: comparing mechanisms for AMPA and GABAA receptors. *Curr. Opin. Pharmacol.* 20:102–108. http://dx.doi.org/10.1016/j.coph.2014.11.011

Mi, H., A. Muruganujan, and P.D. Thomas. 2013. PANTHER in 2013: modeling the evolution of gene function, and other gene attributes, in the context of phylogenetic trees. *Nucleic Acids Res.* 41:D377–D386. http://dx.doi.org/10.1093/nar/gks1118

Neuhofer, D., C.M. Henstridge, B. Dudok, M. Sepers, O. Lassalle, I. Katona, and O.J. Manzoni. 2015. Functional and structural deficits at accumbens synapses in a mouse model of Fragile X. *Front. Cell. Neurosci.* 9:100. http://dx.doi.org/10.3389/fncel.2015.00100

Pehar, M., and L. Puglielli. 2013. Lysine acetylation in the lumen of the ER: a novel and essential function under the control of the UPR. *Biochim. Biophys. Acta.* 1833:686–697. http://dx.doi.org/10.1016/j.bbamcr.2012.12.004

Pehar, M., K.J. O'Riordan, M. Burns-Cusato, M.E. Andrzejewski, C.G. del Alcazar, C. Burger, H. Scrable, and L. Puglielli. 2010. Altered longevity-assurance activity of p53:p44 in the mouse causes memory loss, neurodegeneration and premature death. *Aging Cell.* 9:174–190. http://dx.doi.org/10.1111/j.1474-9726.2010.00547.x

Pehar, M., M.C. Jonas, T.M. Hare, and L. Puglielli. 2012a. SLC33A1/AT-1 protein regulates the induction of autophagy downstream of IRE1/XBP1 pathway. *J. Biol. Chem.* 287:29921–29930. http://dx.doi.org/10.1074/jbc.M112.363911

Pehar, M., M. Lehnus, A. Karst, and L. Puglielli. 2012b. Proteomic assessment shows that many endoplasmic reticulum (ER)-resident proteins are targeted by N(epsilon)-lysine acetylation in the lumen of the organelle and predicts broad biological impact. *J. Biol. Chem.* 287:22436–22440. http://dx.doi.org/10.1074/jbc.C112.362871

Pehar, M., M.H. Ko, M. Li, H. Scrable, and L. Puglielli. 2014. P44, the 'longevity-assurance' isoform of P53, regulates tau phosphorylation and is activated in an age-dependent fashion. *Aging Cell.* 13:449–456. http://dx.doi.org/10.1111/acel.12192

Peng, Y., M. Li, B.D. Clarkson, M. Pehar, P.J. Lao, A.T. Hillmer, T.E. Barnhart, B.T. Christian, H.A. Mitchell, B.B. Bendlin, et al. 2014. Deficient import of acetyl-CoA into the ER lumen causes neurodegeneration and propensity to infections, inflammation, and cancer. *J. Neurosci.* 34:6772–6789. http://dx.doi.org/10.1523/JNEUROSCI.0077-14.2014

Pietrocola, F., L. Galluzzi, J.M. Bravo-San Pedro, F. Madeo, and G. Kroemer. 2015. Acetyl coenzyme A: a central metabolite and second messenger. *Cell Metab.* 21:805–821. http://dx.doi.org/10.1016/j.cmet.2015.05.014

Prasad, A., D. Merico, B. Thiruvahindrapuram, J. Wei, A.C. Lionel, D. Sato, J. Rickaby, C. Lu, P. Szatmari, W. Roberts, et al. 2012. A discovery resource of rare copy number variations in individuals with autism spectrum disorder. *G3 (Bethesda).* 2:1665–1685. http://dx.doi.org/10.1534/g3.112.004689

Prasun, P., S. Young, G. Salomons, A. Werneke, Y.H. Jiang, E. Struys, M. Paige, M.L. Avantaggiati, and M. McDonald. 2015. Expanding the clinical spectrum of mitochondrial citrate carrier (SLC25A1) deficiency: facial dysmorphism in siblings with epileptic encephalopathy and combined D,L-2-hydroxyglutaric aciduria. *JIMD Rep.* 19:111–115. http://dx.doi.org/10.1007/8904_2014_378

Pucilowska, J., J. Vithayathil, E.J. Tavares, C. Kelly, J.C. Karlo, and G.E. Landreth. 2015. The 16p11.2 deletion mouse model of autism exhibits altered cortical progenitor proliferation and brain cytoarchitecture linked to the ERK MAPK pathway. *J. Neurosci.* 35:3190–3200. http://dx.doi.org/10.1523/JNEUROSCI.4864-13.2015

Sanders, S.J., A.G. Ercan-Sencicek, V. Hus, R. Luo, M.T. Murtha, D. Moreno-De-Luca, S.H. Chu, M.P. Moreau, A.R. Gupta, S.A. Thomson, et al. 2011. Multiple recurrent de novo CNVs, including duplications of the 7q11.23 Williams syndrome region, are strongly associated with autism. *Neuron.* 70:863–885. http://dx.doi.org/10.1016/j.neuron.2011.05.002

Shi, L., and B.P. Tu. 2015. Acetyl-CoA and the regulation of metabolism: mechanisms and consequences. *Curr. Opin. Cell Biol.* 33:125–131. http://dx.doi.org/10.1016/j.ceb.2015.02.003

Speed, H.E., M. Kouser, Z. Xuan, J.M. Reimers, C.F. Ochoa, N. Gupta, S. Liu, and C.M. Powell. 2015. Autism-associated insertion mutation (InsG) of Shank3 exon 21 causes impaired synaptic transmission and behavioral deficits. *J. Neurosci.* 35:9648–9665. http://dx.doi.org/10.1523/JNEUROSCI.3125-14.2015

Szklarczyk, D., A. Franceschini, S. Wyder, K. Forslund, D. Heller, J. Huerta-Cepas, M. Simonovic, A. Roth, A. Santos, K.P. Tsafou, et al. 2015. STRING v10: protein-protein interaction networks, integrated over the tree

of life. *Nucleic Acids Res.* 43(D1):D447–D452. http://dx.doi.org/10.1093/nar/gku1003

Thevenon, J., M. Milh, F. Feillet, J. St-Onge, Y. Duffourd, C. Jugé, A. Roubertie, D. Héron, C. Mignot, E. Raffo, et al. 2014. Mutations in SLC13A5 cause autosomal-recessive epileptic encephalopathy with seizure onset in the first days of life. *Am. J. Hum. Genet.* 95:113–120. http://dx.doi.org/10.1016/j.ajhg.2014.06.006

Wellen, K.E., G. Hatzivassiliou, U.M. Sachdeva, T.V. Bui, J.R. Cross, and C.B. Thompson. 2009. ATP-citrate lyase links cellular metabolism to histone acetylation. *Science.* 324:1076–1080. http://dx.doi.org/10.1126/science.1164097

Xu, M., J.S. Nagati, J. Xie, J. Li, H. Walters, Y.A. Moon, R.D. Gerard, C.L. Huang, S.A. Comerford, R.E. Hammer, et al. 2014. An acetate switch regulates stress erythropoiesis. *Nat. Med.* 20:1018–1026. http://dx.doi.org/10.1038/nm.3587